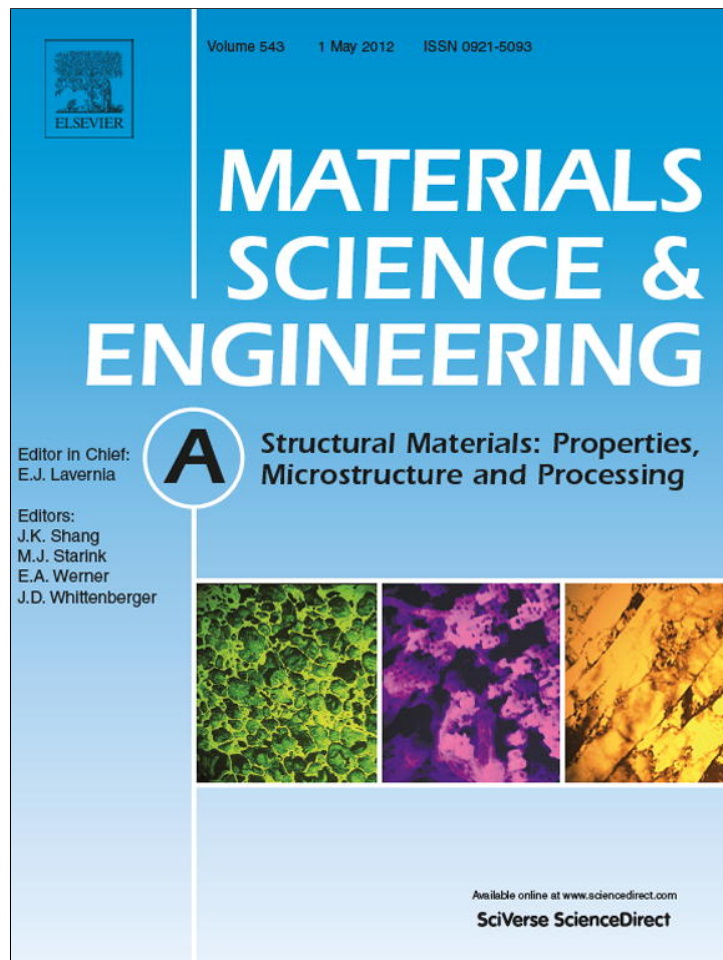


Provided for non-commercial research and education use.
Not for reproduction, distribution or commercial use.



This article appeared in a journal published by Elsevier. The attached copy is furnished to the author for internal non-commercial research and education use, including for instruction at the authors institution and sharing with colleagues.

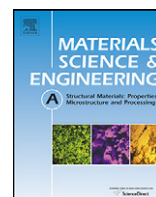
Other uses, including reproduction and distribution, or selling or licensing copies, or posting to personal, institutional or third party websites are prohibited.

In most cases authors are permitted to post their version of the article (e.g. in Word or Tex form) to their personal website or institutional repository. Authors requiring further information regarding Elsevier's archiving and manuscript policies are encouraged to visit:

<http://www.elsevier.com/copyright>

Contents lists available at [SciVerse ScienceDirect](http://www.sciencedirect.com)

Materials Science and Engineering A

journal homepage: www.elsevier.com/locate/msea

Strain rate sensitivity studies in an ultrafine-grained Al–30 wt.% Zn alloy using micro- and nanoindentation

Nguyen Q. Chinh^{a,*}, Tamás Csanádi^a, Tivadar Győri^a, Ruslan Z. Valiev^b, Boris B. Straumal^{c,d}, Megumi Kawasaki^{e,f}, Terence G. Langdon^{e,g}

^a Department of Materials Physics, Eötvös Loránd University, H-1117 Budapest, Hungary

^b Institute of Physics of Advanced Materials, Ufa State Aviation Technical University, 12 K. Marx str., Ufa 450000, Russia

^c Institute of Solid State Physics, Russian Academy of Sciences, Chernogolovka, Moscow District 142432, Russia

^d Karlsruhe Institute of Technology (KIT), Institute of Nanotechnology, Hermann-von-Helmholtz-Platz 1, 76344 Eggenstein-Leopoldshafen, Germany

^e Departments of Aerospace & Mechanical Engineering and Materials Science, University of Southern California, Los Angeles, CA 90089-1453, USA

^f Division of Materials Science and Engineering, Hanyang University, 17 Haengdang-dong, Seongdong-gu, Seoul 133-791, South Korea

^g Materials Research Group, School of Engineering Sciences, University of Southampton, Southampton SO17 1BJ, UK

ARTICLE INFO

Article history:

Received 23 December 2011

Received in revised form 18 February 2012

Accepted 20 February 2012

Available online 3 March 2012

Keywords:

Ultrafine-grained materials

Grain boundary sliding

Wetted boundaries

Strain rate sensitivity

Micro and nanoindentation

ABSTRACT

The characteristics of plastic deformation of an ultrafine-grained (UFG) Al–30 wt.% Zn alloy were investigated using depth-sensing micro- and nanoindentation. Emphasis was placed on the effects of grain boundaries and the unusually high strain rate sensitivity. It is shown that there is a close relationship between enhanced strain rate sensitivity and ductility in this UFG material and this is associated with grain boundary sliding and enhanced diffusion along the Al/Al grain boundaries which appear to be wetted by Zn-rich layers.

© 2012 Elsevier B.V. All rights reserved.

1. Introduction

It is now well established that bulk ultrafine-grained (UFG) materials may be achieved by using severe plastic deformation (SPD) techniques such as equal-channel angular pressing (ECAP) or high-pressure torsion (HPT) [1–3]. As a consequence of the severe deformation, the UFG materials generally have reasonably saturated microstructures with a steady-state dislocation density [4]. Furthermore, in the UFG materials the role of the grain boundaries is generally enhanced in post-SPD deformation processes thereby leading to high strength [5,6]. There is direct evidence suggesting that grain boundary sliding (GBS) may occur more easily at room temperature (RT) in UFG metals [7–9]. At the same time, the UFG materials produced by SPD typically exhibit very low – about only 5–10% – tensile ductility at ambient temperature due to an exhaustion in the work hardening capacity. In addition, the low ductility is correlated with the extremely low strain rate sensitivity (SRS) of only about 0.01–0.03 characterizing these materials [10].

Because the low ductility limits the practical applications, several attempts have been made to improve the tensile ductility of the UFG materials. As the ductility is controlled mainly by work hardening and/or the strain rate sensitivity [9], it was possible to successfully improve the tensile ductility of some UFG metals up to ~40–50% by enhancing the work hardening [11–13]. Recently, it was demonstrated that SPD is capable of increasing the room temperature ductility of an HPT-processed UFG Al–30 wt.% Zn alloy leading to unusually high elongations up to 150% while maintaining an enhanced strength [9]. Thus, the objective of the present investigation was to study and analyze the main plastic characteristics which delineate the high ductility of this UFG Al–30 wt.% Zn alloy. In order to demonstrate the unusual mechanical properties of the alloy, the mechanical characteristics are compared also with results obtained for UFG pure Al processed by HPT.

2. Experimental materials and procedures

As-cast high purity (4N) Al and an Al–30 wt.% Zn alloy were homogenized at 500 °C for 1 and 5 h, respectively. Disks having thicknesses of ~0.8 mm with diameters of 10 mm for Al and 20 mm for Al–30 wt.% Zn were prepared for the subsequent HPT processing. The disks were processed by HPT at room temperature under

* Corresponding author. Tel.: +36 1 3722845; fax: +36 1 3722811.

E-mail address: chinh@metal.elte.hu (N.Q. Chinh).

an imposed pressure of 6.0 GPa. The straining was continued up to a total of 5 turns at a rotation speed of 1 rpm. Samples for investigation were cut from the HPT disks at a distance of approximately one-half radius from the center where this distance corresponds to a shear strain of ~ 6 [3]. The microstructure of the Al–30 wt.% Zn alloy after HPT contained equiaxed ultrafine Al grains having an average size of ~ 380 nm with smaller Zn grains located mainly at the triple junctions of the Al grains [9]. The microstructure of the HPT-processed pure Al consisted also of equiaxed grains having an average size of ~ 1.2 μm where this grain size is consistent with that reported earlier for high-purity Al using ECAP [14,15] and HPT [16].

The mechanical properties were studied using both depth-sensing micro- and nanoindentation tests controlled by computer. The data of depth and load were recorded as a function of time. The microindentation measurements were carried out using a Shimadzu machine with Vickers microindenter operating under a force, F , that increased linearly with time, t , through an imposed loading rate between 0.25 and 70 mN s^{-1} . It may be estimated from an earlier analysis [17] that the equivalent strain rate, $\dot{\epsilon}_{eq}$, around the edge of the indenter at the end of the indentation process is proportional to the loading rate. Applying microindentation at a maximum load of 2000 mN, the equivalent strain rate, $\dot{\epsilon}_{eq}$, was varied between 6.25×10^{-5} and $1.75 \times 10^{-2} \text{ s}^{-1}$. The size of the indenter patterns was ~ 50 – 100 μm , covering at least 5000 grains so that quasi-macroscopic behavior may be observed. The reported microhardness values are the averages of at least 5 individual measurements. The error bars on these average values were estimated as $<5\%$. The equivalent yield strengths, σ_{eq} , were taken as one-third of the hardness values in the present analysis.

Nanoindentation was applied to monitor the effect of the grain boundaries. The nanohardness measurements were carried out using a UMIS nanoindentation device with a Berkovich indenter and applying maximum loads of 0.5 and 1 mN with loading rates of 10^{-2} and $2 \times 10^{-2} \text{ mN s}^{-1}$. A series of 400 indentations was recorded with the indents arranged in a 20×20 matrix with a neighbor-spacing of 20 μm at a given maximum load and loading rate. The maximum indentation depth, h_{max} , was between 60 and 180 nm depending on the applied maximum load and also on the local hardness.

3. Experimental results and discussion

Recently [4,8] it was shown for face-centered cubic (f.c.c.) metals with ultrafine-grained structure that plastic deformation during uniaxial compression takes place at the saturation flow stress which corresponds to a dynamic equilibrium between the formation and annihilation of dislocations. The strain rate, $\dot{\epsilon}$, for the

saturation state may be described through the relationship generally applied in steady-state creep [18]:

$$\dot{\epsilon} = A \frac{DGb}{kT} \left(\frac{\sigma}{G}\right)^n \cdot \left(\frac{b}{d}\right)^p, \quad (1)$$

where A is a dimensionless mechanism-dependent constant, D is the diffusion coefficient, G is the shear modulus, b is the Burgers vector, k is Boltzmann's constant, T is the absolute testing temperature, n is the stress exponent, and p is the inverse grain size exponent for the grain size, d . The diffusion coefficient, D , is given as $D = D_0 \exp(-Q/RT)$, where D_0 is a frequency factor, Q is the appropriate activation energy for the diffusive process and R is the universal gas constant. In addition, the strain rate sensitivity, m , characterizing the deformation process is the reciprocal of the stress exponent ($m = 1/n$). Using the parameters m and Q , Eq. (1) may be rewritten as:

$$\dot{\epsilon} = K_1 \cdot \frac{\sigma^{1/m}}{T} \cdot \exp\left(-\frac{Q}{RT}\right), \quad (2)$$

where K_1 is a microstructure-dependent constant for a selected metal having a constant grain size. Assuming a constant strain rate, Eq. (2) may be expressed as

$$\frac{\sigma}{T^m} = K_2 \cdot \exp\left(\frac{mQ}{RT}\right), \quad (3)$$

where K_2 is another constant.

It follows from Eqs. (2) and (3) that the values of m and Q can be determined from the slope of a straight line fit to the $\ln \sigma - \ln \dot{\epsilon}$ data at a selected temperature and the slope of a straight line fit to the $(\ln \sigma - m \cdot \ln T) - 1/T$ data at a constant strain rate, respectively. Fig. 1 shows such a set of $\ln \sigma_{eq} - \ln \dot{\epsilon}_{eq}$ and $(\ln \sigma_{eq} - m \cdot \ln T) - 1/T$ relationships using the equivalent strain rate, $\dot{\epsilon}_{eq}$, and equivalent stress, σ_{eq} , obtained by microindentation using a Vickers indenter. Fig. 1 allows a calculation of the experimental values of m and Q , respectively, for the two HPT-processed UFG samples.

It is apparent that the quantities obtained by indentation ($m \approx 0.03$ and $Q \approx 87$ kJ/mol) for UFG Al are in good agreement with the values reported earlier from compression testing ($m \approx 0.03$ and $Q \approx 82$ kJ/mol) [8]. Although the value of m for UFG Al is very small, it is typical of the low values of the strain rate sensitivities generally recorded in f.c.c. metals deformed at low temperatures [10,19,20]. In addition, the measured activation energy is very close to the value of ~ 84 kJ/mol anticipated for grain boundary diffusion in pure Al [21].

For the UFG Al–30 wt.% Zn alloy, the value of the strain rate sensitivity ($m \approx 0.22$) is unusually high and this is consistent with the high ductility at room temperature where elongations to failure were achieved of up to more than 150%. However, the experimentally determined activation energy of 65 kJ/mol is lower than the

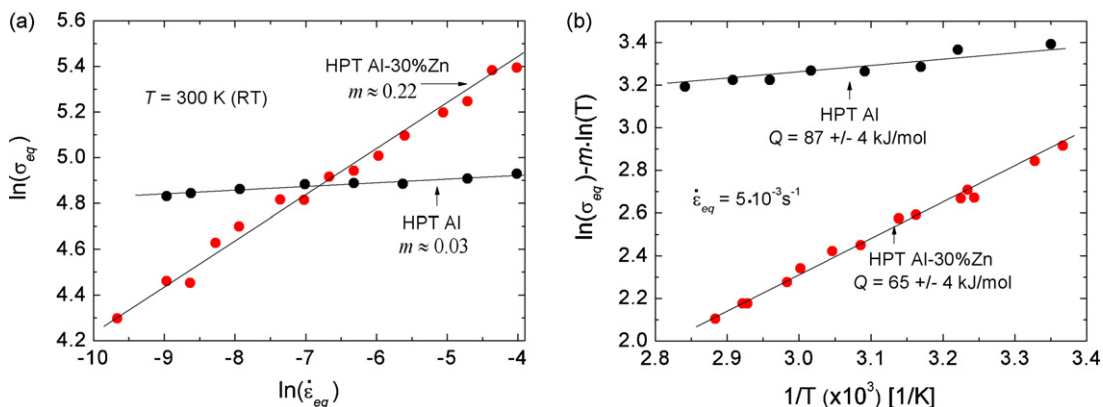


Fig. 1. An evaluation of (a) the strain rate sensitivity, m , and (b) the activation energy, Q , for HPT-processed, UFG Al and Al–30 wt.% Zn alloy.

values for self-diffusion in Al (142 kJ/mol [21]), self-diffusion in Zn (92 kJ/mol [21]) or grain boundary diffusion in Al (84 kJ/mol [21]) and, therefore, it is necessary to examine the reason for this discrepancy.

It is noted that the frequency factors, D_0 , for the latter three diffusion coefficients are similar and lie between $\sim 1.3 \times 10^{-5}$ and $\sim 1.7 \times 10^{-4} \text{ m}^2 \text{ s}^{-1}$ [21]. Assuming a similar frequency factor for the diffusion process in the HPT-processed Al–30 wt.% Zn alloy, and taking $D = D_0 \cdot \exp(-Q/RT)$ with $Q = 65 \text{ kJ/mol}$ at $T = 300 \text{ K}$ for flow at RT, it follows that the diffusion coefficient may be estimated as having a value between $\sim 1.2 \times 10^{-17}$ and $\sim 1.6 \times 10^{-16} \text{ m}^2 \text{ s}^{-1}$. It is important to note that this value of D for the HPT-processed Al–30 wt.% Zn alloy is about three orders of magnitude higher than the coefficient ($\sim 10^{-19} \text{ m}^2 \text{ s}^{-1}$) for aluminum self-diffusion along the Al/Al grain boundaries [21]. Nevertheless, the estimated value of D for the HPT-processed Al–30 wt.% Zn alloy correlates reasonably with the measured diffusivity ($\sim 10^{-15} \text{ m}^2 \text{ s}^{-1}$) for Zn along Al/Al grain boundaries [22,23]. This suggests the occurrence of grain boundary sliding whereby the super-ductility observed in the HPT-processed Al–30 wt.% Zn alloy at room temperature is apparently controlled mainly by Zn diffusion along the Al/Al grain boundaries.

It is important to note that the reason for this unusual behavior can be attributed to the development of thin layers of a Zn-rich grain boundary phase. In this model, the high ductility state corresponds to the UFG structure where a large fraction of the Al/Al boundaries are wetted with thin Zn-rich layers formed during the HPT process. The question of the wetting of the Al/Al grain boundaries by the layers of Zn phase was first addressed in earlier work [24]. It was observed that solid Zn incompletely wets the Al/Al grain boundaries between 200 and 270 °C. Thus, the contact angles between Zn particles and Al/Al grain boundaries remain non-zero even after long anneals. Later careful measurements of these contact angles in Al–10 at.% Zn polycrystals between 190 and 258 °C demonstrated that the maximum, mean and minimum contact angle slowly decreased with decreasing temperature [25]. A linear extrapolation to lower temperatures leads to the expectation that all Al/Al grain boundaries below $\sim 125 \text{ °C}$ should be fully wetted by the Zn layers. It was also observed earlier that HPT of Al–Zn alloys accelerates the phase transformations and produces phases which are stable at the temperature of the HPT processing [26]. The HPT-driven formation of the (thin or thick) Zn-rich wetting layers, which are in equilibrium at room temperature, is the physical explanation for the phenomena observed in this work. Further microstructural investigations are now planned to check and to explain the origin of these unusual Zn-rich layers. Concerning the mechanisms of the flow processes in this HPT-processed Al–30 wt.% Zn alloy, a significant contribution of grain boundary sliding should be taken into

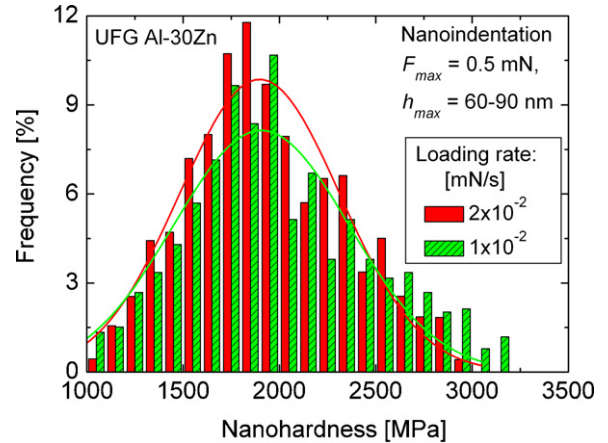


Fig. 2. The distribution of nanohardness obtained at maximum load of 0.5 mN with two different loading rates on UFG Al–30 wt.% Zn alloy. The solid lines indicate the Gauss fit of the spectra.

account. This contribution to the total deformation process was measured earlier as 50–60% [9].

In order to evaluate the role of the grain boundaries, nanoindentation measurements were made in different conditions, thereby causing plastic deformation at different scales. A series of 400 nanoindentation measurements was made at a very low maximum load of 0.5 mN, so that the size of the indenter pattern was about equal to the average grain size of the UFG Al–30 wt.% Zn alloy. In this case it is most probable that the measurements were carried out on individual grains in both UFG Al and Al–30 wt.% Zn. Fig. 2 shows the distribution of the nanohardness obtained for different loading rates on the UFG Al–30 wt.% Zn sample. It can be seen that these nanohardness-spectra are almost the same, thereby indicating that the nanohardness of UFG Al–30 wt.% Zn is not sensitive to the loading rate. This means that when only one grain is deformed in UFG Al–30 wt.% Zn the strain rate sensitivity is very low so that the deformation process or the nanohardness is not sensitive to the strain rate.

Increasing the maximum load, a series of 400 nanoindentation measurements was made at a higher maximum load of 1 mN so that the size of the indenter pattern was $\sim 1\text{--}1.5 \mu\text{m}$, which is about 3–4 times the average grain size of the UFG Al–30 wt.% Zn alloy so that the indenter pattern covers a group of $\sim 5\text{--}7$ grains. The experimental results shown in Fig. 3a reveal that in this case the distribution of the nanohardness obtained on the UFG Al–30 wt.% Zn alloy becomes sensitive to the loading rate. Fitting Gauss functions for the measured spectra and taking the peak value,

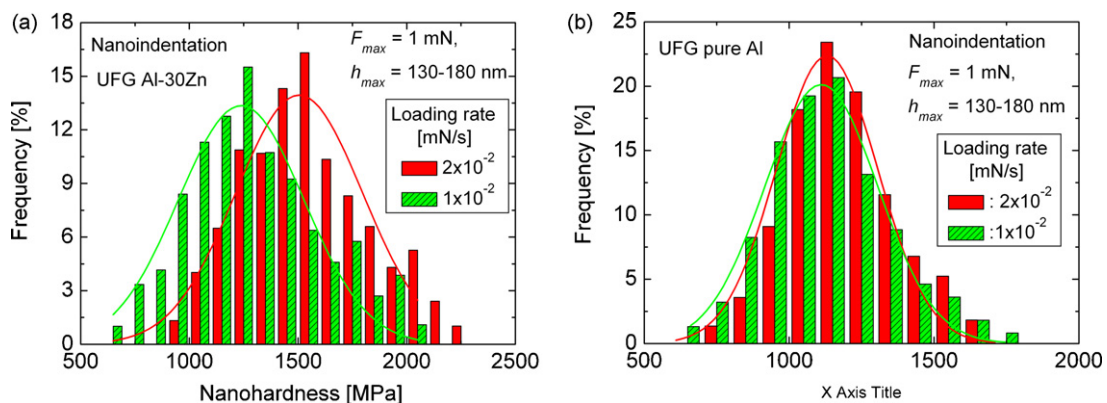


Fig. 3. The distribution of nanohardness obtained at maximum load of 1 mN with two different loading rates on (a) UFG Al–30 wt.% Zn alloy and (b) UFG pure Al. The solid lines indicate the Gauss fit of the spectra.

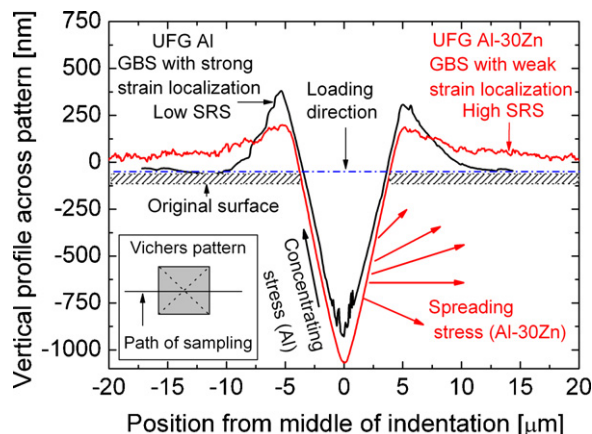


Fig. 4. Plot of the vertical profiles across the centers of the Vickers patterns showing the qualitative difference in GBS of UFG pure Al and UFG Al–30 wt.% Zn and schematically demonstrating the correlation between GBS and the strain rate sensitivity.

similar to the results obtained by microindentation shown in Fig. 1a, an unusually high strain rate sensitivity of $m \approx 0.25$ was estimated also for the deformation process during nanoindentation. Therefore, the results of nanoindentation show unambiguously that, when a group of grains is plastically deformed in the UFG Al–30 wt.% Zn alloy, the role of the grain boundaries should be taken into account. The nanoindentation results presented in Fig. 3b confirm the low strain rate sensitivity of UFG pure Al as the nanohardness distribution of this material appears insensitive to the loading rate. These results obtained by nanoindentation qualitatively support the data determined by microindentation as shown in Fig. 1a.

It should be emphasized that, despite a significant difference between the strain rate sensitivities of UFG Al and UFG Al–30 wt.% Zn, there is no quantitative difference in the contribution of GBS for these two materials. This contribution to the total deformation process has been measured as 50–60% for both materials [7–9]. However, considering the shapes of the pile-ups around the Vickers patterns during microindentation, there is a significant qualitative difference in the flow process for these two materials. Fig. 4 plots typical vertical profiles across the Vickers microhardness patterns for the two metals. These plots reveal that the pile-ups in UFG pure Al are short-range and appear sharp only in the immediate vicinity of the Vickers pattern whereas in the UFG Al–30 wt.% Zn alloy the pile-ups are long-range and spread over relatively long distances from the Vickers pattern. This difference is due to the significantly higher mobility of the grain boundaries in the Al–30 wt.% Zn alloy so that the UFG material becomes super-ductile at room temperature. Furthermore, this difference in the flow process correlates directly with the values of the SRS of these two materials, as demonstrated schematically in Fig. 4. Thus, in the UFG Al–30 wt.% Zn alloy the relatively high SRS prevents the formation of high pile-ups around the Vickers pattern and this is analogous to conventional tensile testing where strain (or stress) fails to concentrate locally thereby precluding the formation of any necking. Instead, the pile-ups in the alloy spread over large areas and thereby they homogenize the deformation and permit the super-ductility of this alloy. Physically, the higher SRS of UFG Al–30 wt.% Zn hinders more effectively the local deformation in the vicinity of the Vickers pattern where the strain and the strain rate are the highest.

4. Summary and conclusions

1) The characteristics of room temperature plastic deformation taking place in ultrafine-grained pure Al and Al–30 wt.% Zn alloy

were investigated and analyzed using depth-sensing indentation.

- 2) The results of micro- and nanoindentation measurements reveal unusually high strain rate sensitivity in the Al–30 wt.% Zn alloy and a significant role of the grain boundaries due to grain boundary sliding in these UFG materials. The present results demonstrate the importance of an enhancement in diffusion along the grain boundaries which promotes flow by GBS and leads to an increased ductility in the Al–30 wt.% Zn alloy.
- 3) The results demonstrate the beneficial improvement in ductility that follows from the enhanced role of the grain boundaries in a UFG Al alloy after processing by severe plastic deformation. Accordingly, the results suggest a new and alternative procedure for developing ductility in UFG materials processed using SPD procedures.

Acknowledgments

This work was supported by the Hungarian Scientific Research Fund (OTKA) under Grants No. K81360, K67692 (NQC), by the Russian Foundation for Basic Research under grants 10-02-00086 and 11-08-90439 (BBS), by the Russian Ministry for Education and Science, by the National Science Foundation of the United States under Grant No. DMR-0855009 (MK and TGL) and by the European Research Council under ERC Grant Agreement No. 267464-SPDMETALS (TGL). The European Union and the European Social Fund provided financial support for this project under Grant Agreement No. TÁMOP 4.2.1./B-09/1/KMR-2010-0003.

References

- [1] R.Z. Valiev, R.K. Islamgaliev, I.V. Alexandrov, Prog. Mater. Sci. 45 (2000) 103.
- [2] R.Z. Valiev, T.G. Langdon, Prog. Mater. Sci. 51 (2006) 881.
- [3] A.P. Zhilyaev, T.G. Langdon, Prog. Mater. Sci. 53 (2008) 893.
- [4] N.Q. Chinh, T. Csanádi, J. Gubicza, T.G. Langdon, Acta Mater. 58 (2010) 5015.
- [5] Y.T. Zhu, X.Z. Liao, Nat. Mater. 3 (2004) 351.
- [6] R.Z. Valiev, Nat. Mater. 3 (2004) 511.
- [7] N.Q. Chinh, P. Szommer, Z. Horita, T.G. Langdon, Adv. Mater. 18 (2006) 34.
- [8] N.Q. Chinh, P. Szommer, T. Csanádi, T.G. Langdon, Mater. Sci. Eng. A 434 (2006) 326.
- [9] R.Z. Valiev, M.Y. Murashkin, A. Kilmetetov, B. Straumal, N.Q. Chinh, T.G. Langdon, J. Mater. Sci. 45 (2010) 4718.
- [10] M.A. Meyer, A. Mishra, D.J. Benson, JOM 58 (4) (2006) 41.
- [11] Y.H. Zhao, J.F. Bingert, X.Z. Liao, B.Z. Cui, K. Han, A.V. Sergueeva, A.K. Mukherjee, R.Z. Valiev, T.G. Langdon, Y.T. Zhu, Adv. Mater. 18 (2006) 2949.
- [12] Y. Zhao, T. Topping, J.F. Bingert, J.J. Thornton, A.M. Danglewicz, Y. Li, W. Liu, Y. Zhou, E.J. Lavernia, Adv. Mater. 20 (2008) 3028.
- [13] P. Xue, B.L. Xiao, Z.Y. Ma, Mater. Sci. Eng. A 532 (2012) 106.
- [14] Y. Iwahashi, Z. Horita, M. Nemoto, T.G. Langdon, Acta Mater. 45 (1997) 4733.
- [15] Y. Iwahashi, Z. Horita, M. Nemoto, T.G. Langdon, Acta Mater. 46 (1998) 3317.
- [16] C. Xu, Z. Horita, T.G. Langdon, Acta Mater. 55 (2007) 203.
- [17] N.Q. Chinh, J. Gubicza, Zs Kovács, J. Lendvai, J. Mater. Res. 19 (2004) 31.
- [18] T.G. Langdon, J. Mater. Sci. 41 (2006) 597.
- [19] H.S. Kim, Y. Estrin, Appl. Phys. Lett. 79 (2001) 4115.
- [20] J. Chen, Y.N. Shi, K. Lu, J. Mater. Res. 20 (2005) 2955.
- [21] H.J. Frost, M.F. Ashby, Deformation-Mechanism Maps: The Plasticity and Creep of Metals and Ceramics, Pergamon Press, Oxford, UK, 1982.
- [22] H. Mehrer (Ed.), Diffusion in Solid Metals and Alloys. Landolt-Börnstein, vol. 26, Springer, Berlin, 1990.
- [23] I. Kaur, W. Gust, L. Kosma, Handbook of Interphase and Grain Boundary Diffusion, Ziegler Press, Stuttgart, 1989.
- [24] B. Straumal, R. Valiev, O. Kogtenkova, P. Zieba, T. Czeppe, E. Bielanska, M. Faryna, Acta Mater. 56 (2008) 6123.
- [25] S.G. Protasova, O.A. Kogtenkova, B.B. Straumal, P. Zieba, B. Baretzky, J. Mater. Sci. 46 (2011) 4349.
- [26] B.B. Straumal, B. Baretzky, A.A. Mazilkin, F. Philipp, O.A. Kogtenkova, M.N. Volkov, R.Z. Valiev, Acta Mater. 52 (2004) 4469.